nature neuroscience

Grid cells require excitatory drive from the hippocampus

Tora Bonnevie[1], Benjamin Dunn[1], Marianne Fyhn[1,3], Torkel Hafting[1,3], Dori Derdikman[1,3], John L Kubie[2], Yasser Roudi[1], Edvard I Moser[1] & May-Britt Moser[1]

To determine how hippocampal backprojections influence spatially periodic firing in grid cells, we recorded neural activity in the medial entorhinal cortex (MEC) of rats after temporary inactivation of the hippocampus. We report two major changes in entorhinal grid cells. First, hippocampal inactivation gradually and selectively extinguished the grid pattern. Second, the same grid cells that lost their grid fields acquired substantial tuning to the direction of the rat's head. This transition in firing properties was contingent on a drop in the average firing rate of the grid cells and could be replicated by the removal of an external excitatory drive in an attractor network model in which grid structure emerges by velocity-dependent translation of activity across a network with inhibitory connections. These results point to excitatory drive from the hippocampus, and possibly other regions, as one prerequisite for the formation and translocation of grid patterns in the MEC.

The hippocampus and entorhinal cortex are part of the brain's map of local space. The first component of this representation was discovered more than 40 years ago, when it had been shown that hippocampal neurons have location-specific firing properties[1]. The origin of the hippocampal place signal remained elusive until the last decade, when cells with spatial firing correlates were identified one synapse upstream, in the MEC[2–5]. The predominant cell type in the MEC network is the grid cell, which fires in a matrix-like hexagonal pattern that tessellates the entire space visited by the animal[3]. Grid cells fire at constant periodic positions irrespective of changes in the animal's speed and direction, and their firing patterns are maintained in the absence of visual input[3], suggesting that the cells use self-motion information to encode the animal's position in the environment[3,6]. This relationship to path integration, together with the strict periodicity of the grid pattern, has pointed to grid cells as the metric component of the entorhinal-hippocampal spatial map[4,6]. In conjunction with head-direction cells[7,8] and border cells[9,10], the grid cells form an invariant representation of local space in which similarities and differences in firing preferences of local cell pairs are maintained across environments[10,11].

Less is known about the mechanisms by which grid cells interact with place cells. Place fields may be generated in the hippocampus by mechanisms that involve linear summation of impulses from grid cells with a range of spatial frequencies[6,12–14] or competitive learning among inputs with random differences in firing locations[15–19]. In the reverse direction, grid cells may also depend on place cells[20–23], but the potential role of hippocampal backprojections in grid formation remains poorly understood. One possibility is that place cells store associations between locations and configurations of external landmarks such that the same activity map can be retrieved on successive occasions[4,20,24]. If this is true, disruption of the output from hippocampal storage sites would not necessarily perturb the grid pattern itself, but without the information from hippocampal storage sites, the grid might drift unpredictably within and between trials. An alternative or additional possibility is that hippocampal output participates directly in the formation or maintenance of the grid pattern by providing either spatial input from which grid fields can be formed through Hebbian self organization[22] or modulatory input that is required for maintaining the network in a condition where spatially periodic firing can be generated. To determine whether grid patterns can be expressed in the absence of hippocampal output, we transiently inactivated the hippocampus by local bilateral infusion of the $GABA_A$ receptor agonist muscimol while simultaneously monitoring spatial firing patterns in the superficial layers of the MEC or, in a few instances, the adjacent parasubiculum (**Fig. 1a** and **Supplementary Figs. 1** and **2**).

Previous work using a similar experimental approach has shown that entorhinal firing fields become wider and less stable on a linear track during the first 30 min after hippocampal inactivation at the same time as theta-phase precession is maintained[25]. This early work focused explicitly on the subset of individual firing fields that persisted after the inactivation, and it was not clear whether the periodicity of the grids was retained. Here we recorded neural activity in the hippocampus and MEC while rats foraged for food crumbs in a square enclosure either 1 m or 1.5 m wide in which two-dimensional spatial periodicity could be detected.

RESULTS

Hippocampal inactivation

We tested the effect of hippocampal output on firing patterns of grid cells in eight rats by local infusion of the $GABA_A$ receptor agonist 5-aminomethyl-3-hydroxyisoxazole (muscimol) through cannulae implanted at the dorsal pole of each rat's hippocampus (**Fig. 1a** and **Supplementary Figs. 1** and **2**; see **Supplementary Fig. 3** for experiments with fluorophore-conjugated muscimol (FCM)[26]). The infusion was

[1]Kavli Institute for Systems Neuroscience and Centre for the Biology of Memory, Norwegian Brain Centre, Norwegian University of Science and Technology (NTNU), Trondheim, Norway. [2]Department of Cell Biology, State University of New York Downstate Medical Center, Brooklyn, New York, USA. [3]Present addresses: Department of Molecular Biosciences, University of Oslo, Kristine Bonnevies hus, Oslo, Norway (M.F. & T.H.) and Technion, Israel Institute of Technology, Rappaport Faculty of Medicine, Bat Galim, Haifa, Israel (D.D.). Correspondence should be addressed to M.-B.M. (maybm@ntnu.no) or E.I.M. (edvard.moser@ntnu.no).

Received 16 August 2012; accepted 13 December 2012; published online 20 January 2013; doi:10.1038/nn.3311

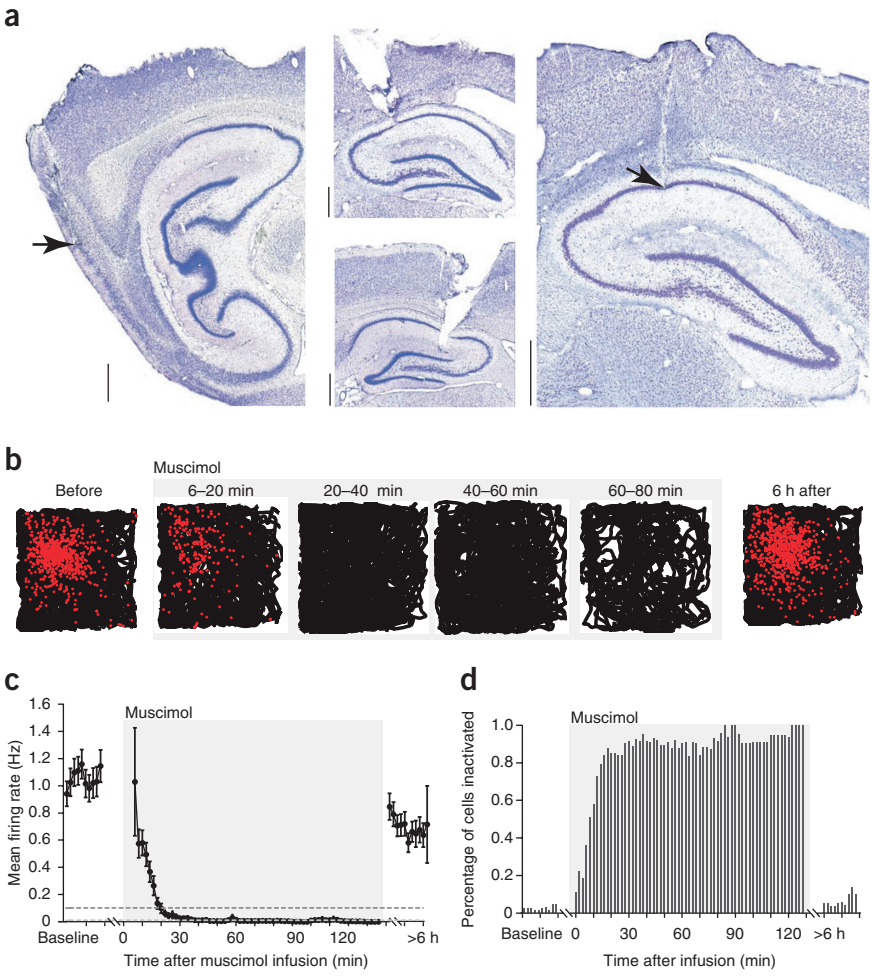

Figure 1 Muscimol-induced inactivation of the dorsal hippocampus. (**a**) Sagittal brain sections showing positions of tetrodes in the MEC (left) and cannulae and tetrodes in the hippocampus (middle and right, respectively). The locations of the tetrode tips are indicated by arrows. The anteromedial-posterolateral distance between the cannulae and tetrodes in the hippocampus is 2.2 mm. Scale bars, 1 mm. (**b**) Trajectory (black) with superimposed spike positions (red) for a representative place cell before and after infusion of the GABAergic agonist muscimol (gray shading indicates presence of muscimol) into the hippocampus. The cell is completely silenced within 20 min. (**c**) Mean firing rate (± s.e.m.) before and after muscimol infusion (all cells in this analysis were hippocampal pyramidal cells). Time $t = 0$ indicates the start of infusion. (**d**) Percentage of the entire cell sample that fired less than 1% of the baseline average in trial blocks before and after muscimol infusion.

followed by a rapid decrease in the firing rate of all principal cells recorded in the dorsal CA1 region, ~2.2 mm posterior and lateral to the infusion site (82 cells, all of which were place cells; **Fig. 1b**). Within 20 min, the rates had dropped to less than 1% of the baseline rate in 79% of the recorded cells (**Fig. 1c**,**d**). Inactivation of the hippocampus had only minimal impact on the behavior of the rats (**Supplementary Fig. 4**).

Entorhinal cell sample

We recorded a total of 273 well-separated cells in the MEC-parasubiculum of the rats before and after inactivation of the hippocampus. We classified these cells as grid cells ($n = 126$), head-direction cells ($n = 26$), border cells ($n = 7$) or other ($n = 14$) on the basis of the cells' firing patterns before inactivation of the hippocampus (**Supplementary Fig. 5**)[27]. The average rotational symmetry, or grid score[8,27,28], of the cells that passed the criterion for grid cells was 0.90 ± 0.03 (mean ± s.e.m. of 20 min of baseline; grid spacing, 64.2 ± 2.1 cm (mean ± s.e.m.)). Twenty-four of the grid cells and six of the border cells also passed the criterion for head-direction cells. We recorded 80 of the MEC-parasubiculum cells simultaneously with hippocampal cells. The cell sample was biased in that we explicitly searched for grid cells; the high percentage of grid cells is not reflective of the true proportion of such cells in the population[8,27].

Loss of grid structure

The drop in hippocampal firing rates was accompanied by a gradual loss of spatial periodicity in the time-averaged activity maps of the grid cells (**Fig. 2a** and **Supplementary Fig. 6**). We observed grid patterns during the first 20–30 min after infusion of muscimol, but the locations of the spikes became progressively more dispersed. Using T_0 as the time when muscimol infusion ended, we found that among the MEC-parasubiculum cells that passed the grid-cell criterion in the baseline trial, 54.9% passed the criterion between T_{10} and T_{20}, and 25.2% passed between T_{30} and T_{160} (**Fig. 2b**). The grid scores of these cells dropped from an average of 0.84 ± 0.03 before the infusion (first 10 min of baseline) to 0.39 ± 0.04 between T_{20} and T_{30} and to 0.13 ± 0.02 between T_{30} and T_{160} (**Fig. 2c**). The scores were significantly reduced for all trial blocks ($t > 6.2$, $P < 0.001$; paired t-test), but the mean score remained above the 95th percentile value for the shuffled distribution (0.184) until 30–40 min after infusion (**Fig. 2c**). The grid scores continued to decrease after this in layers II and III of the MEC, as well as in the parasubiculum (grid scores of 0.16 ± 0.24, 0.12 ± 0.03 and 0.10 ± 0.03, respectively, between T_{30} and T_{160}; $F_{2,142} = 1.18$, $P = 0.31$; one-way analysis of variance), with final values remaining slightly above the average (50th percentile) of the shuffled distribution (–0.169). When we retested the rats 6 h or 24 h after infusion, the CA1 firing rates had returned to baseline values (**Fig. 1**), and the grid scores (0.71 ± 0.04) had recovered.

Grids do not reappear in dynamic correlation maps

We then investigated whether grid patterns disappear from time-averaged rate maps because the phase and orientation of the grids become unstable when output from hippocampal storage sites is blocked. We postulated that for a drifting grid, spatial periodicity should be visible if the time window for the correlation analysis is made sufficiently short. To test this, we generated spike-triggered autocorrelation maps in which we plotted all spikes during a 10-s time window after each spike of the trial relative to the location of the preceding reference spike (**Fig. 3a**,**b**). These dynamic autocorrelation maps showed clear grid patterns in the baseline trial, but after muscimol infusion, spatial periodicity was no more visible than it was in the time-averaged maps. The decrease in grid scores was apparent with time windows of 10 s (from 0.16 ± 0.02 to –0.08 ± 0.01 between T_{30} and T_{160}; $t_{142} = 10.2$, $P < 0.001$) and 60 s (from 0.26 ± 0.03 to –0.11 ± 0.01; $t_{142} = 12.6$, $P < 0.001$). With the 10-s window, only 2.1% of the cells passed the

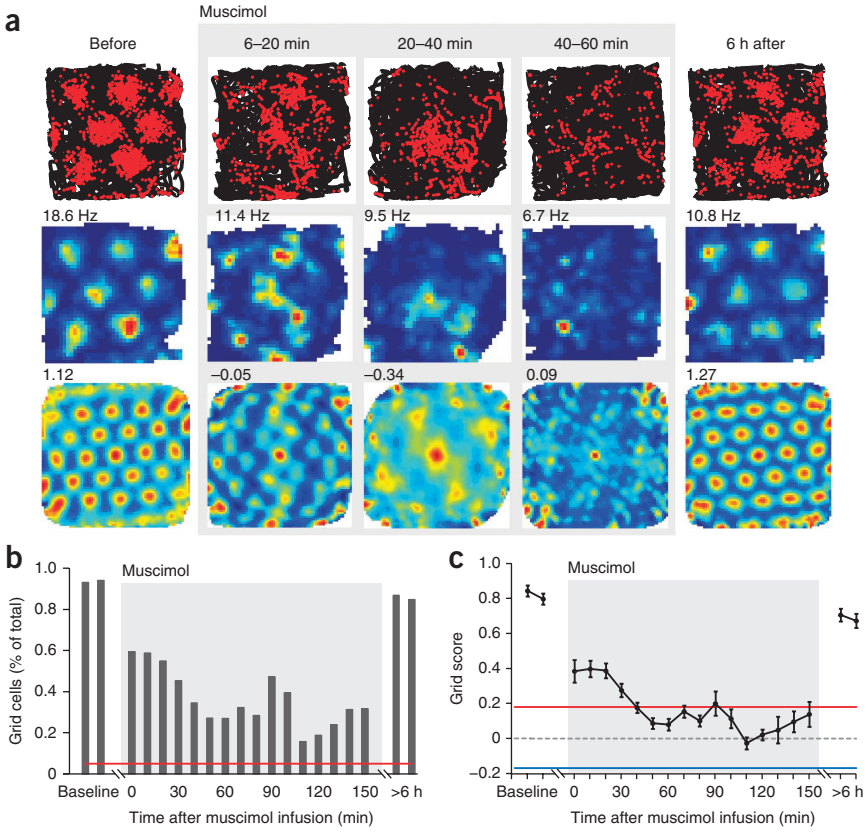

Figure 2 Disruption of entorhinal grid structure after inactivation of the hippocampus. (**a**) Trajectory with spike positions (top), rate map (middle) and autocorrelation map (bottom) for successive trial blocks in a grid cell after muscimol infusion in the hippocampus. Rate maps and autocorrelation maps are color coded with cold (blue) and warm (red) colors indicating low and high rates and correlation values, respectively. The correlation colors are scaled to the observed range. Peak rates and grid scores are indicated over the rate maps and the autocorrelation maps, respectively. Baseline and 6-h maps were recorded over a 20-min period. Pixels not covered are white. The scale of the autocorrelation diagrams is twice the scale of the rate maps (side lengths of 200 cm compared to 100 cm, respectively). For additional examples, see **Supplementary Figure 6**. (**b**) Percentage of cell samples that passed the 95th percentile criterion for grid cells in 10-min trial blocks before and after hippocampal muscimol infusion. Percentages refer to the total number of cells that passed the criterion in an analysis of the entire baseline period (20 min). The red line indicates the chance value (5%). (**c**) Mean grid scores (± s.e.m.) for trial blocks of 10 min starting 20 min before infusion. Grid scores measure the degree of sixfold rotational symmetry in the spatial autocorrelation map of the cell. The red line indicates the 95th percentile of a distribution of shuffled spike times for the same cells (400 permutations); the blue line indicates the 50th percentile.

criterion for grid cells; with the 60-s window, 9.1% of the cells passed the criterion. These observations provide evidence against the drift hypothesis but cannot rule out that grids were present in even shorter time blocks for which sampling was too limited to detect periodicity in the autocorrelograms.

To target the shortest time intervals, we used spike-triggered cross-correlations. Such analyses can be performed for pairs of grid cells on path segments not longer than the space between the grid vertices of the cell pair, which can be any fraction of the cells' individual grid spacing. For the baseline trials, we found reliable cross-correlation peaks for blocks as short as 1 s (**Fig. 3c,d**). After muscimol infusion, these peaks were substantially diminished (the first-order spatial autocorrelation, or spatial coherence, of the cross-correlogram decreased from 0.62 ± 0.01 (mean ± s.e.m.) during baseline to 0.32 ± 0.01 between T_{30} and T_{160}; $t_{854} = 28.9$, $P < 0.001$), and there was a clear decrease in stability of the cross-correlograms (pixel-by-pixel correlation, 0.50 ± 0.01 for baseline trial 1 compared to baseline trial 2; 0.27 ± 0.01 for baseline compared to between T_{20} and T_{30} and 0.14 ± 0.01 for baseline compared to between T_{30} and T_{160}; all analyses used time windows of 1 s; **Fig. 3d**). The remaining stability between T_{30} and T_{160} was not stronger with a 1-s window than with longer windows (10-s window, 0.15 ± 0.01; 60 s window, 0.15 ± 0.01; same number of pixels). The cross-correlation analysis cannot rule out that individual grid cells maintained independently drifting grid patterns that were too short to be expressed in dynamic autocorrelation maps, but the analyses do suggest that the spatial-phase relationship of the grid-cell population was disrupted, even for very short path segments.

Increased directional tuning

The breakdown of the grid pattern was accompanied by the emergence of directional tuning in previously nondirectional grid cells (**Fig. 4** and **Supplementary Fig. 6**). Thirty-two of 43 nondirectional grid cells (74%) became directional in MEC layer II, 25 out of 37 cells (68%) became directional in MEC layer III and 32 out of 39 cells (82%) became directional in the parasubiculum. The length of the mean firing-rate vector of these cells increased from 0.10 ± 0.01 (mean ± s.e.m.) during the baseline trial to 0.25 ± 0.01 during the inactivation period (T_{30}–T_{160}; $t_{118} = 12.8$, $P < 0.001$; **Fig. 4b,d**). The directional tuning of cells that satisfied the criterion for head-direction cells in the baseline trial was less affected (0.41 ± 0.03 during baseline; 0.49 ± 0.03 between T_{30} and T_{160}; $t_{54} = 4.86$, $P < 0.001$; **Fig. 4c**). In these cells, the increase in tuning was confined to cells with weak direction tuning at the outset (bottom quartile, from 0.25 to 0.41; top quartile, from 0.67 to 0.68). The preferred firing direction of cells with head-direction tuning in the baseline trial was only moderately stable between baseline and T_{30} (absolute change in preferred firing direction, 48.8° ± 17.6° (circular mean angle ± 99% confidence interval)) and between T_{30} and the end of the trial (44.0° ± 18.6°). The directional drift during the inactivation was not significantly larger, however, than between baseline and recovery 6 h or 24 h after muscimol infusion (36.6° ± 20.1°; $F_{1,99} = 0.50$, $P > 0.50$; Watson-Williams two-sample test for circular data). In grid cells that developed directional tuning, the directional preferences were even less stable than for the cells that were directional in the baseline trial (change in preferred direction from first to last 10-min trial block with significant directional tuning, 68.8° ± 14.9°; $F_{1,153} = 7.63$, $P < 0.02$; Watson-Williams two-sample test). This difference could, however, reflect the weaker directional tuning of the newly direction-tuned cells.

Contribution of firing rate

The loss of grid structure was accompanied by a reduction in the firing rates of the grid cells (**Fig. 5**). The grid structure and firing rate

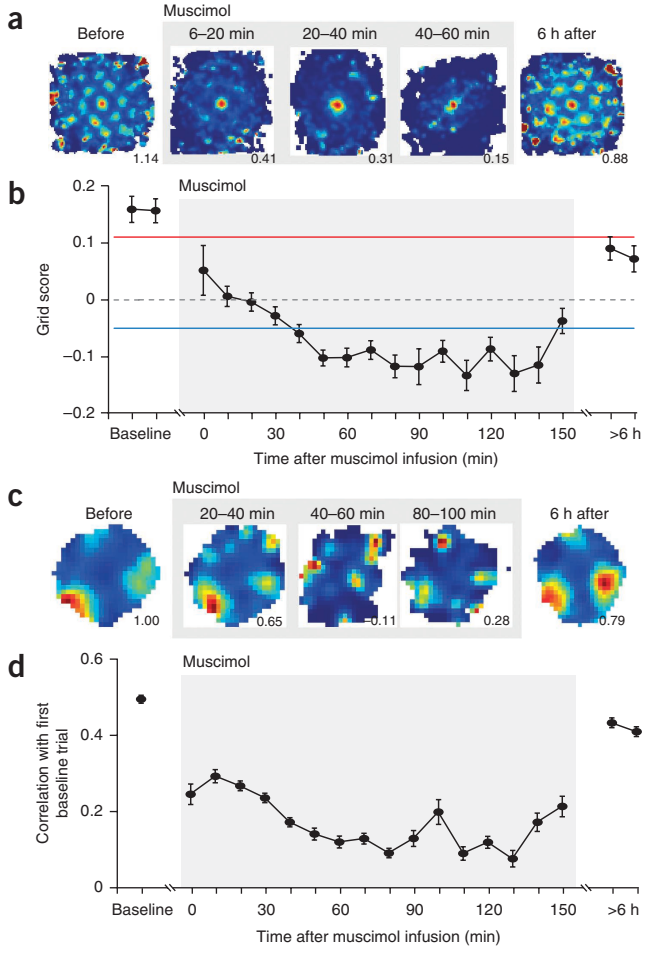

Figure 3 Disappearance of the grid pattern in dynamic maps. (**a**) Spike-triggered (dynamic) spatial autocorrelation maps showing the grid structure for 10-s time windows referenced to the location of each spike. One map is shown for each time block before and after muscimol infusion for a representative cell. The width of each map is 200 cm. The correlations are color coded and range from 0 (dark blue) to the maximum correlation value indicated at the bottom right of each map (dark red). Grid scores are indicated for each map. Baseline and 6-h maps were recorded over a 20-min period. (**b**) Grid scores (mean ± s.e.m.) of dynamic autocorrelation maps. Time is measured from the end of the hippocampal infusion. The 95th percentile criterion is indicated by the red line; the blue line indicates the 50th percentile. Note the disappearance of the grid structure after hippocampal inactivation despite the use of a moving reference point. (**c**) Spike-triggered (dynamic) spatial crosscorrelogram showing the effect of hippocampal inactivation on the spatial-phase relationship in successive trial blocks in a representative pair of simultaneously recorded grid cells (regular rate maps and autocorrelation maps for the same cells are shown in **Supplementary Fig. 6**). Each map shows the distribution of correlation between the first cell's firing rate at the trigger location and the second cell's firing rate at all relative locations visited during the subsequent 1-s interval. The correlations are color coded as in **a**. The width of each map is 60 cm (30 cm away from the origin). Cross-correlation values are indicated for each map (baseline and 6-h maps are 20 min). Note that the spatial-phase relationship of the two grid cells is disrupted by inactivation of the hippocampus, suggesting that the original spatial structure of the grid cells is abolished even at time intervals as short as 1 s. (**d**) Correlation between dynamic cross-correlation maps in the first 10-min block of baseline recording and in subsequent 10-min blocks (second block of baseline, muscimol infusion and recovery; means ± s.e.m.).

reached minimal values at approximately the same time, ~40 min after muscimol infusion (**Figs. 1c**,**d** and **5a**). The decrease in firing rates leveled off at 58.0% ± 4.1% of baseline (mean rate for T_{30}–T_{160} ± s.e.m.; $t_{142} = 10.3$, $P < 0.001$; paired t-test). There was no significant difference in rate change between directional and nondirectional grid cells (71.1% ± 11.0% and 55.3% ± 4.4%, respectively, of baseline between T_{30} and T_{160}; $t_{141} = 1.4$; $P > 0.10$; independent-samples t-test **Fig. 5a**), and we found similar decreases for grid cells in the MEC and parasubiculum (57.7% ± 5.5% and 58.4% ± 5.6%, respectively; $t_{141} = 0.08$) and in layers II and III of the MEC (65.9% ± 7.9% and 47.7% ± 7.1%, respectively; $t_{94} = 1.7$, independent-samples t-test). The lowest grid scores during muscimol infusion were associated with the largest rate reductions (**Fig. 5b**; correlation between the grid score between T_{30} and T_{160} and the proportional decrease in mean firing rate of all simultaneously recorded grid cells (r) = 0.49, $P < 0.01$). In trials with small rate decrements (upper quartile of the rate distribution between T_{30} and T_{160}), the grid scores dropped to an average of 0.26 ± 0.06, which was above the 95th percentile of grid scores after shuffling (**Supplementary Fig. 7a**). On average, 19 of the 39 grid cells recorded in this subset of trials continued to pass the 95th percentile grid-cell criterion. In trials with more substantial rate decrements (bottom quartile), the grid scores dropped to 0.05 ± 0.02 (**Supplementary Fig. 7b**), and only 1 of the 22 cells passed the grid-cell criterion. The decrease in firing rate was also predictive of the increase in directional tuning or mean vector length (r = –0.45, P = 0.02: **Fig. 5b**). After hippocampal inactivation, there was only a marginal drop in the firing rate of cells that were head-direction tuned in the baseline trial (absolute rate, $t_{25} = 2.3$, $P = 0.03$; rate normalized to baseline, $t_{25} = 1.4$, $P = 0.18$; **Fig. 5a**).

The loss of grid structure at the lowest firing rates was not caused by an inability to detect symmetry in grid cells with low firing rates. When we downsampled the rate maps from the baseline trial to the spike frequencies of the trials after infusion, the grid scores dropped only marginally (**Fig. 5c**,**d**). The increase in directional modulation with reduced rate was also not an artifact of poor sampling, as the mean vector lengths of the grid cells were nearly unaffected by downsampling to the rates after infusion (**Fig. 5c**,**d**).

Remaining nonperiodic spatial firing

We next investigated whether nonperiodic spatial firing was retained after inactivation of the hippocampus. Muscimol infusion caused a significant drop in the spatial coherence (first-order spatial autocorrelation) of the firing fields (from 0.60 ± 0.02 during baseline to 0.31 ± 0.01 between T_{30} and T_{160}; $t_{142} = 16.5$, $P < 0.001$; paired t-test), but the values generally remained higher than the chance value obtained for coherence in the shuffled data (0.20; $t_{142} = 7.7$, $P < 0.001$ between T_{30} and T_{160}; single-sample t-test; **Fig. 6a**,**b**). We found a similar effect for the spatial correlation between rate maps during baseline and after muscimol infusion. This correlation was significantly larger than the correlation between the data after infusion and the shuffled baseline data (T_{20}–T_{30}, $r = 0.22 \pm 0.02$; $t_{142} = 9.60$, $P < 0.001$; T_{30}–T_{160}, $r = 0.11 \pm 0.01$; $t_{142} = 7.45$, $P < 0.001$; paired t-test). Rate-map correlations between the first and second half of the trial block decreased from 0.61 ± 0.02 during baseline to 0.18 ± 0.01 between T_{30} and T_{160}, which was still above the chance value ($t_{142} = 14.3$, $P < 0.001$; **Fig. 6c**). The spatial modulation persisted when we restricted the analysis to the grid cells with the lowest grid scores during the inactivation (bottom quartile of grid scores between T_{30} and T_{160}; spatial coherence, 0.30 ± 0.03; $t_{35} = 3.7$, $P = 0.001$; single-sample t-test; spatial stability, 0.15 ± 0.02; $t_{35} = 6.7$, $P < 0.001$; paired t-test). Spatial structure was similarly retained in the small number of border cells in the cell sample; none of these cells was markedly affected by inactivation of the hippocampus (**Supplementary Fig. 8**).

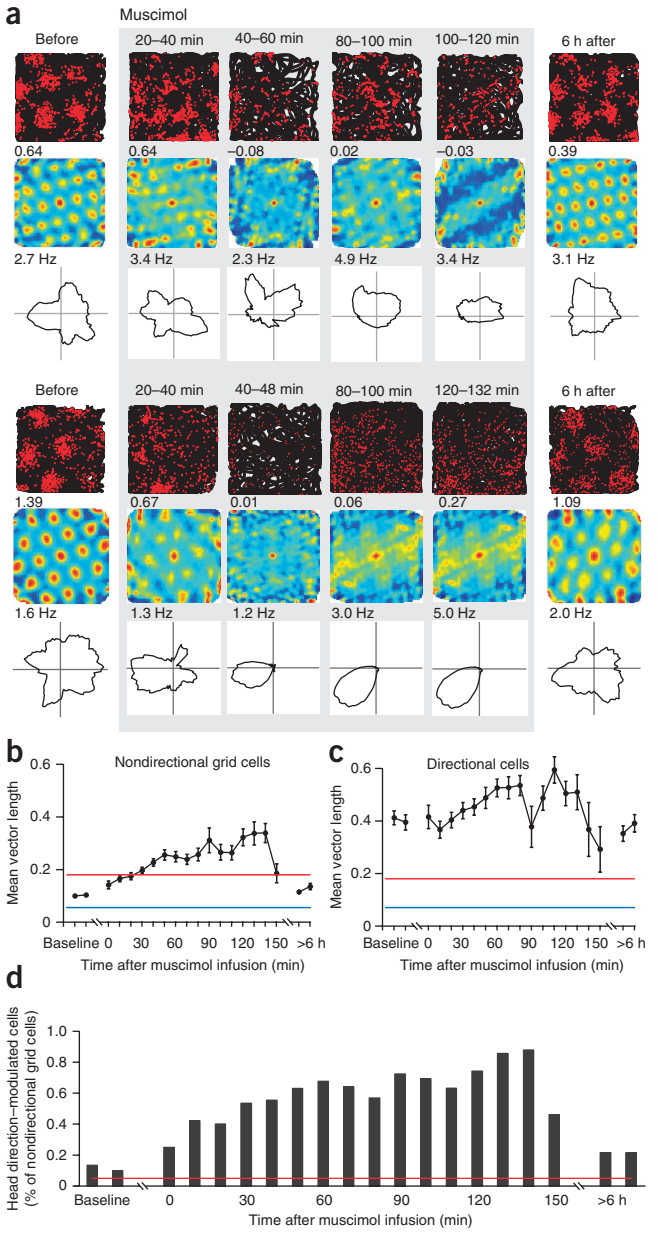

Figure 4 Loss of grid structure leads to directional tuning. (**a**) Development of directional tuning after the disruption of grid structure in two example cells (with the top three rows showing one cell and the bottom three rows showing the other cell). The top two rows for each cell show the trajectory with spike locations and the spatial autocorrelation maps, respectively. The grid scores are indicated above the autocorrelation maps. The bottom row for each cell shows polar plots of firing rate as a function of head direction. The peak firing rate is indicated over each plot. For additional examples, see **Supplementary Figure 6**. (**b**,**c**) Development of mean vector length after hippocampal muscimol infusion (means ± s.e.m.), with results shown for all grid cells that were nondirectional in the baseline trial (**b**) and all cells with direction modulation in the baseline trial (**c**). The gray area indicates the presence of muscimol. The red line indicates the 95th percentile value for mean vector length in the corresponding shuffled distributions; the blue line indicates the 50th percentile. (**d**) Percentage of initially nondirectional grid cells that passed the 95th percentile criterion for head-direction cells in trial blocks after hippocampal infusion of muscimol. Percentages refer to the total number of cells that passed the criterion in an analysis of the entire baseline period (20 min). The gray box indicates the presence of muscimol. The red line indicates the chance value (5%).

Preserved theta activity

We next investigated whether the loss of grid structure, and the increase in directional modulation, reflected a global change in entorhinal network state. The spatial periodicity of grid cells is expressed under conditions in which theta activity predominates in hippocampal and medial entorhinal electroencephalography (EEG) readings[25]. To determine whether the grid cells we studied here disappeared because of perturbation of local theta oscillations, we investigated the power spectra for each cell, as well as field EEG readings recorded in parallel with firing of individual neurons.

After inactivation of the hippocampus, theta activity continued to predominate the entorhinal EEG readings, although at reduced power (**Fig. 7a**,**b**), and the majority of the grid cells remained moderately theta modulated (**Fig. 7c**). The number of grid cells with a peak in the theta frequency band, defined as those cells for which the spectral power in the 6–11 Hz band was at least threefold greater than the mean power in the 1–125 Hz band, decreased from 86% during baseline to 49% during muscimol infusion (T_{30}–T_{160}; $Z = 6.73$, $P < 0.001$; binomial test), whereas the number of grid cells with theta power identical to or greater than the mean power between 1 Hz and 125 Hz (still large enough to appear as a peak in the theta region) was only reduced from 98% to 97% ($Z = 0.39$, $P = 0.35$; binomial test). The inactivation caused a significant reduction in the absolute power of the theta frequency band in EEG readings from the MEC (baseline compared to after muscimol infusion, $t_{29} = 3.56$, $P = 0.001$; paired t-test), as could be expected when the mean firing rate decreases. This reduction was slower and smaller when the theta power was normalized by the power across the entire 1–125 Hz frequency band (baseline compared to after muscimol infusion, $t_{30} = 6.31$, $P < 0.001$, paired t-test; **Fig. 7d**). There was a slight decrease in the peak frequency in the theta band of spectra on the basis of field EEG readings (before infusion, 8.1 ± 0.09 Hz (mean ± s.e.m.); after infusion, 7.8 ± 0.07 Hz; $t_{29} = 3.03$, $P = 0.005$; paired t-test) or interspike intervals of individual neurons (before infusion, 8.4 ± 0.09 Hz; after infusion, 8.1 ± 0.08 Hz; $t_{139} = 2.92$, $P < 0.005$; paired t-test). In general, the peak theta frequency of the autocorrelograms from individual cells was higher than that of the simultaneously recorded local EEG, both in the baseline data (89 out of 140 cells; frequency difference, 0.30 ± 0.08 Hz; $t_{139} = 3.71$, $P < 0.001$; paired t-test) and after muscimol infusion (95 out of 136 cells; frequency difference, 0.35 ± 0.06 Hz; $t_{135} = 6.07$, $P < 0.001$, paired t-test; T_{30}–T_{160}) (**Fig. 7e**). The frequency difference was not altered by muscimol infusion ($Z = 1.1$, binomial test; $t_{143} = 1.1$, paired t-test). The persistence of faster oscillations in individual cells compared to the field signal is consistent with data from linear environments showing that theta-phase precession[29] is preserved during muscimol-induced inactivation of the hippocampus[25].

Computational model

We showed that hippocampal output is necessary for the emergence of grid patterns in the MEC and that without this input the MEC grid cells become head directional. A simple explanation for this change in response properties can be provided using an attractor model of grid cell formation in the MEC. We modeled the inactivation experiment in a continuous attractor model of grid cells that consisted of threshold-linear units arranged on a two-dimensional lattice of 128 × 128 nodes with periodic boundary conditions (a torus[6]). We topographically rearranged grid cells according to their spatial phases[6,12]. Following a previously described model and to mirror realistic stellate-cell networks in the rat entorhinal cortex, we connected the

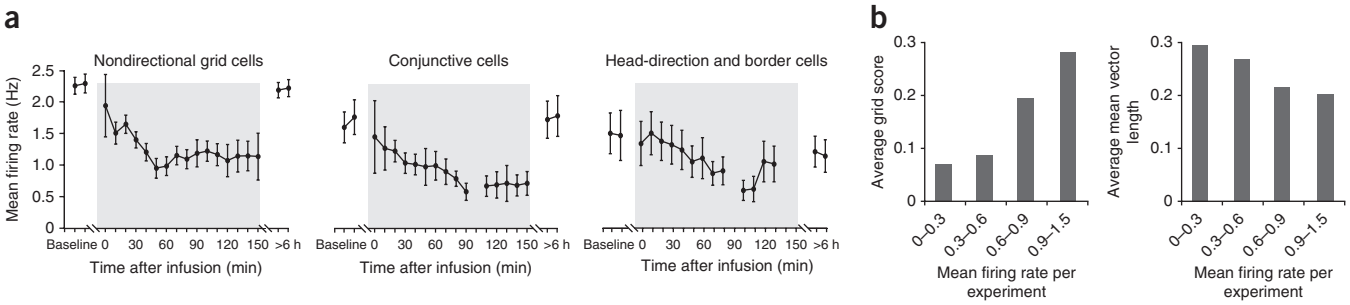

Figure 5 Loss of the grid pattern depends on the decrease in firing rates of grid cells. (**a**) Mean firing rates (± s.e.m.) before and after muscimol infusion for the entire sample of entorhinal cells (left, grid cells with no directional modulation; middle, conjunctive grid and head-direction cells; right, head-direction and border cells combined). (**b**) Relationship between the normalized average firing rate (relative to the baseline rate) and either grid score (left) or mean vector length (right) after hippocampal inactivation (mean values for all simultaneously recorded grid cells are shown). (**c**,**d**) Grid scores and mean vector lengths for the trial before infusion as a function of downsampling of spike numbers. (**c**) Examples of trajectory maps, rate maps and directional plots before and after downsampling (10-min trials). The grid score is indicated above each rate map, and the mean vector length is indicated over each directional plot. (**d**) Line diagram showing the decrease of grid scores and the increase of mean vector length (black and red line, respectively; means ± s.e.m.) as a function of downsampling of data from 10-min blocks of baseline recording. Note that both measures tolerate considerable downsampling well beyond the reduction of firing rates observed after muscimol infusions in the experimental data (dashed line).

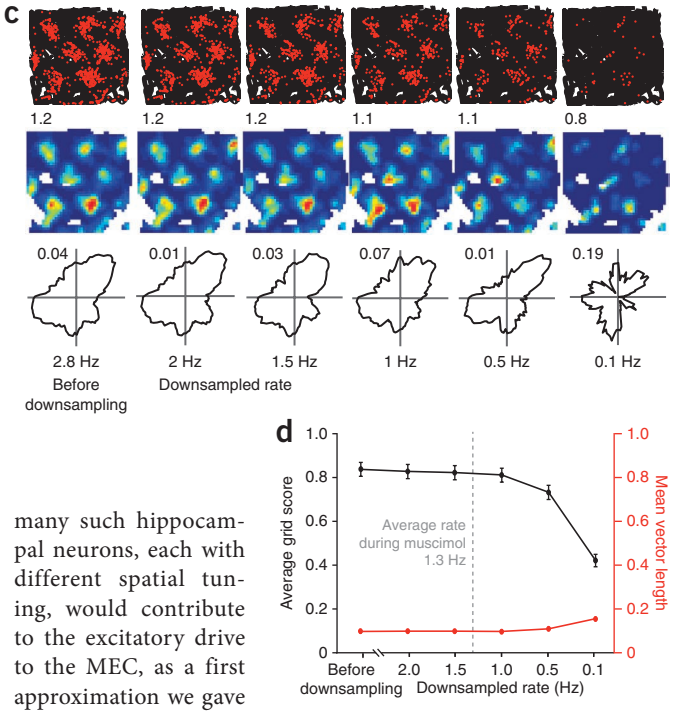

cells to each other using effective inhibitory connections[30,31] without explicitly modeling the inhibitory interneurons. This connectivity had an all-or-none profile; that is, only neurons with grid fields close to each other (distance less than a fixed radius apart) were connected, and the strength of the connection was the same for all connected pairs independent of their distance[31]. As within this network neurons only receive inhibition from each other, to generate activity they need to receive an external excitatory drive. In our model, this excitatory drive represents the activity of neurons in the hippocampus, which directly or indirectly influences the grid network. Because many such hippocampal neurons, each with different spatial tuning, would contribute to the excitatory drive to the MEC, as a first approximation we gave this excitatory drive a constant value. Because of the competitive inhibitory interaction between entorhinal stellate cells, the activity of the network rapidly settles into a hexagonal grid pattern on the two-dimensional neuronal sheet[30,31] (**Fig. 8a** and **Supplementary Video 1**). Once the pattern of activity is generated, it can be translated in the direction of the animal's movement through speed-modulated head-direction input to the grid cells[6,12]. The single-cell response is then the transcription of the pattern of activity over time (**Fig. 8a** and **Supplementary Video 1**). To implement the head-directional input in the model, we assigned a directional preference to each grid cell and assumed that it receives head-directional input tuned to this preferred direction. Furthermore, the connectivity was slightly offset in network space

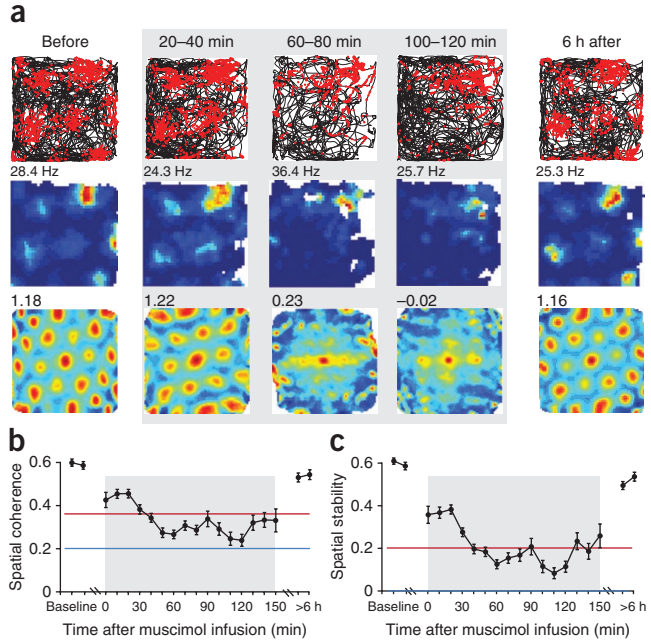

Figure 6 Remaining nonperiodic spatial firing after hippocampal inactivation. (**a**) Localized nonperiodic firing in two example cells after hippocampal muscimol infusions that removed all visible grid structure (from top to bottom, trajectory with spike locations, rate map and autocorrelation map; peak rates and grid scores are indicated). (**b**,**c**) Spatial coherence (**b**) and spatial stability (**c**) of all grid cells from all rats (means ± s.e.m.). Spatial coherence is the average correlation between the firing rate in neighboring bins of the recording box (first-order spatial autocorrelation); spatial stability is the bin-by-bin correlation of firing rates between the first and second half of the trial. The red line indicates the 95th percentile value of the shuffled distribution, and the blue line indicates the chance value (50th percentile). The chance value for spatial stability is 0.

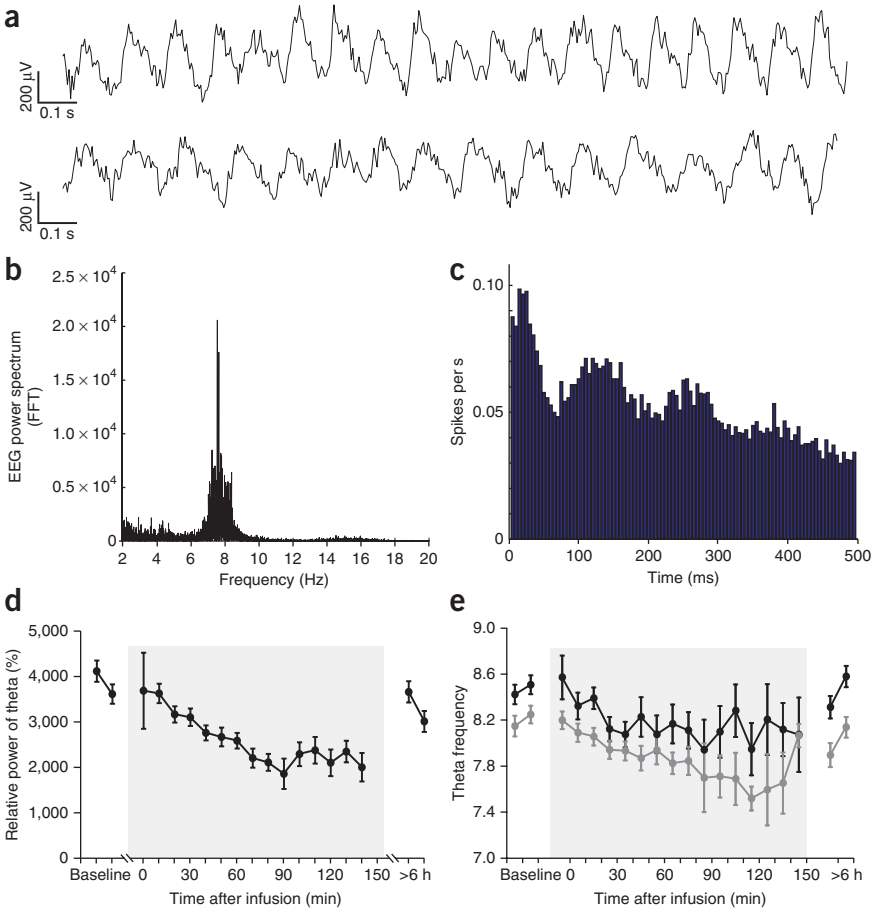

Figure 7 Preserved theta activity during hippocampal inactivation. (**a**) Local entorhinal EEG readings showing 2.0 s of activity during running in the open field before (top) and 30 min after (bottom) hippocampal muscimol infusion. (**b**) Power spectrum showing the persistence of theta activity in entorhinal EEG readings after hippocampal muscimol infusion during a representative trial (T_{30}–T_{160}, 1–125 Hz filter). FFT, fast Fourier transform. (**c**) Spike time autocorrelation diagram showing the persistence of theta modulation (spiking at ~125-ms intervals) in a grid cell after muscimol infusion (T_{30}–T_{160}). (**d**) Relative power of theta activity in entorhinal EEG readings as a function of time after hippocampal muscimol infusion (mean ± s.e.m.). Theta power was normalized by the power in the entire 1–125 Hz band. (**e**) Peak theta frequency of spike-time autocorrelation functions of individual grid cells (autocorrelogram, gray) and theta peak frequency in simultaneously recorded local EEG (black) as a function of time after muscimol infusion (mean ± s.e.m.). Note that individual cells are modulated at a higher theta frequency than the field EEG readings both before and after muscimol infusion, suggesting that phase precession is preserved[25].

according to the preferred direction of each cell[6,12]. The combination of the head-directional input and the offset enables the grid activity on the network to translate with the animal's movement, yielding grid activity at the single-cell level. On the basis of this model, we simulated the hippocampal inactivation experiments to determine how network dynamics in the MEC change. We ran each simulation with a different value for the amplitude of the hippocampal input and left all the head direction–modulated inputs unchanged. For each value of external input, we had the virtual rat navigate nine trials in a virtual environment and monitored the activity of 50 randomly chosen single neurons.

Consistent with the experimental data, the model showed two regimes depending on the strength of the hippocampal input and the resulting firing rates of the grid cells (**Fig. 8b** and **Supplementary Video 1**). For large enough hippocampal inputs, the network showed grid-cell activity through the generation and translation of a grid pattern (**Fig. 8b**,**c**). A substantially different network dynamic occurred when the hippocampal input was small and the firing rates in the MEC were therefore low. In this latter regime, firing was determined primarily by the head-directional input, resulting in an increased length of the mean firing-rate

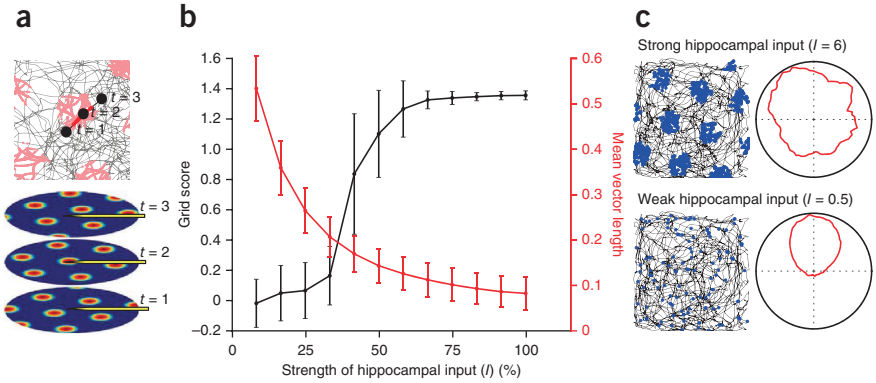

Figure 8 The effect of hippocampus inactivation in an attractor model of grid cells. (**a**) Cartoon showing how the movement of activity across the neuronal sheet (bottom three images) results in the spatially selective firing of a single cell (top image). At time $t = 1$, the pointer is recording from a cell that is currently inactive. From $t = 1$ to $t = 2$, the activity pattern is translated with the movement of the animal such that the indicated cell has an elevated firing rate and is therefore in its spatial field. The cell then leaves its spatial field as the population activity shifts at $t = 3$. **Supplementary Video 1** shows an example of this translation of activity and how it is reflected in single-cell firing. (**b**) Grid scores and mean vector length (mean ± s.e.m.) compared to the strength of external input (I). For large external inputs, high grid scores are achieved through the mechanism described in **a**; see also **Supplementary Video 1**. As the external input is decreased below a critical amount, the activity on the neuronal sheet, even if hexagonal, is not stable in the sense that it is easily distorted (**Supplementary Video 2**). At the single-cell level, therefore, no grid-like activity is present, and the grid scores drop. At the same time, the head-directional input becomes the dominant source of input to the cells, and the neurons show high directional tuning. For each value of external input, we simulated the network when a virtual rat navigated nine experimentally recorded tracks, and each time we took the response of 50 random neurons from the network. The averages and error bars are over these 450 neurons. (**c**) Spike distribution plots and directional tuning curves generated from example cells for the extreme cases of weak hippocampal input (bottom) and strong hippocampal input (top).

vector (**Fig. 8b**,**c**). In contrast to the hippocampal input, which activated all neurons in the same way, the head-direction input at any given time only excited neurons with a preferred firing direction that was similar to the animal's movement. The inhibitory nature of the connections prevented the propagation of activity from these active neurons to the inactive ones, and, with low excitatory input from the hippocampus, neurons with tunings different from the momentary direction of the animal's movement had little or no activity and thus had minimal impact on the network dynamics. Under these conditions, the network did not settle into a stable grid-like activity pattern that was capable of being translated across the network without distortions (**Supplementary Video 2**), no grid pattern was expressed in individual cells and the grid scores dropped toward the chance value (**Fig. 8b**,**c**). These observations are consistent with the experimental data in suggesting that an excitatory drive from the hippocampus, or elsewhere, is necessary for generating and translating the grid pattern in the inhibitory network of the MEC and that head-direction inputs increase their influence on the firing pattern of grid cells in the absence of the excitatory drive. This directional impact would not be expected if grid-like activity were sustained by excitatory interconnections[6,12].

DISCUSSION

It is commonly thought that grid cells are necessary for the formation of place cells. Our results show, conversely, that hippocampal backprojections are necessary for grid structure in the MEC. Hippocampal muscimol infusion abolished nearly all firing in place cells of the dorsal hippocampus. This was followed by a substantial reduction in the average activity of principal cells in the MEC. The spatial periodicity of the grid cells was almost eliminated, and the cells became responsive to head direction. The loss of grid structure and the increase in directional modulation were strongly correlated with the drop in entorhinal firing rates. The effects on spatial periodicity and directional modulation could be replicated by removal of external excitatory drive in an attractor network model in which grid structure emerges by velocity-dependent translation of activity across a network coupled exclusively by inhibitory connections.

It is clear from our data that entorhinal cells cannot normally express grid patterns in the absence of active hippocampal backprojections. Previous studies have indicated that entorhinal cells maintain a certain degree of localized firing after lesions in the hippocampus[2] or during the first 30 min after temporary inactivation of the hippocampus[25], and key features of temporal organization such as theta-phase precession have been shown to be preserved in the subset of moderately preserved firing fields when output from the hippocampus is blocked[25]. Our data confirm these observations but extend them by showing that the spatial periodicity of the entorhinal firing pattern gradually disappears and directional modulation takes over. The persistence of theta rhythmicity and theta-phase precession when the effects of muscimol reach a steady state and minimal grid structure is retained suggest that the disruption of the grid pattern is not caused only by changes in the network state of the MEC.

These data constrain the mechanisms by which hippocampal backprojections might contribute to the formation of grid cells. One idea is that associations between path-integrator coordinates and specific features of the environment are stored in the hippocampus and that sustained feedback from these storage sites prevents accumulation of error in the entorhinal representation of self position[4,20,24]. Perturbation of such feedback would be expected to generate drift in the grid pattern. If the disappearance of grids after muscimol infusion was only caused by drift, grids should reappear in analyses with very short time windows. The continued disruption of autocorrelation and crosscorrelation structure at short intervals makes this possibility unlikely. The finding does not rule out a role for the hippocampus in updating position coordinates but suggests that, independently of such a function, the backprojections are necessary for expression of the grid pattern itself.

How might hippocampal output control the formation of the grid pattern? Our results could be explained if spatial signals from place cells were used as inputs to form the grid pattern[22]. The exact mechanism for such a place-to-grid transformation would need further investigation, however, as place cells may themselves be generated by grid cells. Our model points to an alternative, and perhaps simpler, mechanism. Our simulations showed that in a network in which principal cells are coupled exclusively through all-or-none inhibitory interneurons, such as among stellate cells in layer II of the MEC[30,31], grid cells can only be formed in the presence of steady external excitation. In the brain, such excitation may be provided by hippocampal axons, which probably target grid cells both indirectly through deep layers of the MEC[32,33] and directly through axons from CA2 neurons (Rowland, D.C. *et al. Soc. Neurosci*. Abstract 513.03; 25 November 2011). Similar excitation may be received from other sources, such as the cholinergic inputs from the medial septum, which may be necessary for maintaining normal firing rates in grid cells[34,35]. The excitation may maintain membrane potentials of grid cells sufficiently close to the firing threshold for speed and direction inputs to translate the activity pattern across the local network[6,12,30]. When the excitatory inputs are blocked, this translation may no longer occur. A certain amount of membrane depolarization may also be required for the operation of intracellular mechanisms of grid formation, if they exist; for example, tonic excitation might be required for subthreshold theta oscillations to generate spatially periodic firing[20,21,36,37]. The strong relationship between loss of firing rate and grid structure in the experimental data is consistent with each of these possibilities. The increase in grid directionality, in contrast, is predicted only by the network model and, to our knowledge, not by alternative models[6,12,21,22,38], which agrees with the modular nature of the grid map[39] as well as the observation that grids can be expressed in the absence of theta oscillations[40]. Taken together, the data point to excitation from the hippocampus as one of the conditions for grid formation in the MEC; however, they do not rule out a relationship between grid formation and specific hippocampal firing patterns separate from a possible role for tonic excitation.

The activity of the hippocampal backprojections had a selective effect on grid cells. The continued functional specificity of the head-direction cells is consistent with previous work reporting maintained firing in these cells under circumstances with minimal spatial periodicity in the grid-cell network of the MEC[28,34,35,41]. Our findings add to this work by showing that perturbation of the grid may enhance directional modulation, with directionality developing in cells that did not previously express such preferences. Taken together, the experimental data and network simulations suggest that in the absence of excitatory hippocampal feedback, the recurrent interactions between grid cells break down, and external inputs obtain stronger control of the discharge pattern of the individual grid cells. Such external inputs may include not only head-direction signals from adjacent parahippocampal structures but also, potentially, broadly tuned nonperiodic spatial signals from other input regions such as the postrhinal cortex[2,42]. These broadly tuned inputs may be sufficient to maintain weak nonperiodic firing fields in the MEC cells. One function of excitatory projections from the hippocampus, and other structures, may thus be to enable grid cells to respond primarily to the intrinsic activity of the stellate-cell

network rather than inputs from neighboring regions. Whether the grid-cell network makes such changes between internally and externally driven dynamics under natural conditions, such as during transitions between behavioral states, remains to be determined.

METHODS

Methods and any associated references are available in the online version of the paper.

Note: Supplementary information is available in the online version of the paper.

ACKNOWLEDGMENTS

We thank R. Skjerpeng for programming, M.P. Witter and C.B. Boccara for advice on tetrode locations, M. Mehta and M.P. Witter for discussion, N. Burgess for sharing code for dynamic autocorrelation analyses and A.M. Amundsgård, K. Haugen, K. Jenssen, E. Kråkvik and H. Waade for technical assistance. This work was supported by the Kavli Foundation, a studentship to T.B. from the Faculty of Medicine at NTNU, a Centre of Excellence grant from the Research Council of Norway and an Advanced Investigator Grant to E.I.M. from the European Research Council ('CIRCUIT', grant agreement 232608).

AUTHOR CONTRIBUTIONS

T.B. and M.F. performed the majority of the experiments; T.B. did the majority of the analyses; B.D. and Y.R. did the network simulations; E.I.M. and T.B. wrote the manuscript, except for the computational model (B.D. and Y.R.); and M.-B.M. supervised the project. All authors contributed to discussion and interpretation.

COMPETING FINANCIAL INTERESTS

The authors declare no competing financial interests.

Published online at http://www.nature.com/doifinder/10.1038/nn.3311.
Reprints and permissions information is available online at http://www.nature.com/reprints/index.html.

1. O'Keefe, J. & Dostrovsky, J. The hippocampus as a spatial map. Preliminary evidence from unit activity in the freely-moving rat. *Brain Res.* **34**, 171–175 (1971).
2. Fyhn, M., Molden, S., Witter, M.P., Moser, E.I. & Moser, M.B. Spatial representation in the entorhinal cortex. *Science* **305**, 1258–1264 (2004).
3. Hafting, T., Fyhn, M., Molden, S., Moser, M.B. & Moser, E.I. Microstructure of a spatial map in the entorhinal cortex. *Nature* **436**, 801–806 (2005).
4. Moser, E.I., Kropff, E. & Moser, M.-B. Place cells, grid cells, and the brain's spatial representation system. *Annu. Rev. Neurosci.* **31**, 69–89 (2008).
5. Giocomo, L.M., Moser, M.-B. & Moser, E.I. Computational models of grid cells. *Neuron* **71**, 589–603 (2011).
6. McNaughton, B.L., Battaglia, F.P., Jensen, O., Moser, E.I. & Moser, M.-B. Path integration and the neural basis of the "cognitive map.". *Nat. Rev. Neurosci.* **7**, 663–678 (2006).
7. Taube, J.S., Muller, R.U. & Ranck, J.B. Jr. Head-direction cells recorded from the postsubiculum in freely moving rats. I. Description and quantitative analysis. *J. Neurosci.* **10**, 420–435 (1990).
8. Sargolini, F. *et al*. Conjunctive representation of position, direction, and velocity in entorhinal cortex. *Science* **312**, 758–762 (2006).
9. Savelli, F., Yoganarasimha, D. & Knierim, J.J. Influence of boundary removal on the spatial representations of the medial entorhinal cortex. *Hippocampus* **18**, 1270–1282 (2008).
10. Solstad, T., Boccara, C.N., Kropff, E., Moser, M.B. & Moser, E.I. Representation of geometric borders in the entorhinal cortex. *Science* **322**, 1865–1868 (2008).
11. Fyhn, M., Hafting, T., Treves, A., Moser, M.-B. & Moser, E.I. Hippocampal remapping and grid realignment in entorhinal cortex. *Nature* **446**, 190–194 (2007).
12. Fuhs, M.C. & Touretzky, D.S. A spin glass model of path integration in rat medial entorhinal cortex. *J. Neurosci.* **26**, 4266–4276 (2006).
13. Solstad, T., Moser, E.I. & Einevoll, G.T. From grid cells to place cells: a mathematical model. *Hippocampus* **16**, 1026–1031 (2006).
14. Molter, C. & Yamaguchi, Y. Entorhinal theta phase precession sculpts dentate gyrus place fields. *Hippocampus* **18**, 919–930 (2008).
15. Rolls, E.T., Stringer, S.M. & Elliot, T. Entorhinal cortex grid cells can map to hippocampal place cells by competitive learning. *Network* **17**, 447–465 (2006).
16. de Almeida, L., Idiart, M. & Lisman, J.E. The input-output transformation of the hippocampal granule cells: from grid cells to place fields. *J. Neurosci.* **29**, 7504–7512 (2009).
17. Savelli, F. & Knierim, J.J. Hebbian analysis of the transformation of medial entorhinal grid-cell inputs to hippocampal place fields. *J. Neurophysiol.* **103**, 3167–3183 (2010).
18. Si, B. & Treves, A. The role of competitive learning in the generation of DG fields from EC inputs. *Cogn. Neurodyn.* **3**, 177–187 (2009).
19. Monaco, J.D. & Abbott, L.F. Modular realignment of entorhinal grid cell activity as a basis for hippocampal remapping. *J. Neurosci.* **31**, 9414–9425 (2011); erratum **31**, 11096 (2011).
20. O'Keefe, J. & Burgess, N. Dual phase and rate coding in hippocampal place cells: theoretical significance and relationship to entorhinal grid cells. *Hippocampus* **15**, 853–866 (2005).
21. Burgess, N., Barry, C. & O'Keefe, J. An oscillatory interference model of grid cell firing. *Hippocampus* **17**, 801–812 (2007).
22. Kropff, E. & Treves, A. The emergence of grid cells: intelligent design or just adaptation? *Hippocampus* **18**, 1256–1269 (2008).
23. Sreenivasan, S. & Fiete, I. Grid cells generate an analog error-correcting code for singularly precise neural computation. *Nat. Neurosci.* **14**, 1330–1337 (2011).
24. Samu, D., Erös, P., Ujfalussy, B. & Kiss, T. Robust path integration in the entorhinal grid cell system with hippocampal feed-back. *Biol. Cybern.* **101**, 19–34 (2009).
25. Hafting, T., Fyhn, M., Bonnevie, T., Moser, M.-B. & Moser, E.I. Hippocampus-independent phase precession in entorhinal grid cells. *Nature* **453**, 1248–1252 (2008).
26. Allen, T.A. *et al*. Imaging the spread of reversible brain inactivations using fluorescent muscimol. *J. Neurosci. Methods* **171**, 30–38 (2008).
27. Boccara, C.N. *et al*. Grid cells in pre- and parasubiculum. *Nat. Neurosci.* **13**, 987–994 (2010).
28. Langston, R.F. *et al*. Development of the spatial representation system in the rat. *Science* **328**, 1576–1580 (2010).
29. O'Keefe, J. & Recce, M.L. Phase relationship between hippocampal place units and the EEG theta rhythm. *Hippocampus* **3**, 317–330 (1993).
30. Burak, Y. & Fiete, I.R. Accurate path integration in continuous attractor network models of grid cells. *PLOS Comput. Biol.* **5**, e1000291 (2009).
31. Couey, J.J. *et al*. Recurrent inhibitory circuitry as a mechanism for grid formation. *Nat. Neurosci.* doi:10.1038/nn.3310 (20 January 2013).
32. van Haeften, T., Baks-te-Bulte, L., Goede, P.H., Wouterlood, F.G. & Witter, M.P. Morphological and numerical analysis of synaptic interactions between neurons in deep and superficial layers of the entorhinal cortex of the rat. *Hippocampus* **13**, 943–952 (2003).
33. Kloosterman, F., Van Haeften, T., Witter, M.P. & Lopes Da Silva, F.H. Electrophysiological characterization of interlaminar entorhinal connections: an essential link for re-entrance in the hippocampal-entorhinal system. *Eur. J. Neurosci.* **18**, 3037–3052 (2003).
34. Brandon, M.P. *et al*. Reduction of theta rhythm dissociates grid cell spatial periodicity from directional tuning. *Science* **332**, 595–599 (2011).
35. Koenig, J., Linder, A.N., Leutgeb, J.K. & Leutgeb, S. The spatial periodicity of grid cells is not sustained during reduced theta oscillations. *Science* **332**, 592–595 (2011).
36. Alonso, A. & Klink, R. Differential electroresponsiveness of stellate and pyramidal-like cells of medial entorhinal cortex layer II. *J. Neurophysiol.* **70**, 128–143 (1993).
37. Yoshida, M., Giocomo, L.G. & Hasselmo, M.E. Frequency of subthreshold oscillations at different membrane potential voltages in neurons at different anatomical positions on the dorsoventral axis in the rat medial entorhinal cortex. *J. Neurosci.* **31**, 12683–12694 (2011).
38. Zilli, E.A. & Hasselmo, M.E. Coupled noisy spiking neurons as velocity-controlled oscillators in a model of grid cell spatial firing. *J. Neurosci.* **30**, 13850–13860 (2010).
39. Stensola, H. *et al*. The entorhinal grid map is discretized. *Nature* **492**, 72–78 (2012).
40. Yartsev, M.M., Witter, M.P. & Ulanovsky, N. Grid cells without theta oscillations in the entorhinal cortex of bats. *Nature* **479**, 103–107 (2011).
41. Wills, T.J., Cacucci, F., Burgess, N. & O'Keefe, J. Development of the hippocampal cognitive map in preweanling rats. *Science* **328**, 1573–1576 (2010).
42. Burwell, R.D. & Hafeman, D.M. Positional firing properties of postrhinal cortex neurons. *Neuroscience* **119**, 577–588 (2003).

ONLINE METHODS

Subjects and surgeries. Neuronal activity was recorded from eight male Long-Evans rats (3–5 months old, 350–450 g at implantation and testing) housed individually in transparent Perspex cages (54 cm × 44 cm × 35 cm) with water available *ad libitum*. The rats were kept on a 12-h light, 12-h dark schedule and tested in the dark phase. After surgery, the rats were placed on a food deprivation schedule that kept them at ~90% of their free-feeding body weight. Three of the rats also participated in experiments measuring phase precession on a linear track[25]. Tests on the linear track[25] and in the open field were performed on separate days in these rats.

Before surgery, the rats were anesthetized with Equithesin (1 ml per 250 g body weight, with supplementary doses of 0.3–0.4 ml as needed). The rats were chronically implanted with two microdrives each connected to four tetrodes of twisted 17-µm HM-L–coated platinum-iridium wire[25]. The electrode tips were platinum plated before surgery to reduce electrode impedances to 150–250 kΩ at 1 kHz. One bundle of four tetrodes was implanted in the MEC in all rats (anteroposterior (AP) 0.4–0.5 mm in front of the transverse sinus, mediolateral (ML) 4.5–4.6 mm from the midline and dorsoventral (DV) 1.4–1.8 mm below the dura). These tetrodes were angled 10° in the sagittal plane, with their tips pointing in the anterior direction. Four of the rats received additional tetrodes implanted vertically into the hippocampus (AP 3.5 mm posterior to the bregma, ML 4.5–4.8 mm from the midline and DV 1.4 mm below the dura). The remaining four rats had a second microdrive implanted at the corresponding position in the contralateral MEC. In addition to the tetrodes, all rats received implants of two 26-ga cannulae (C315G, Plastics One), one above each hippocampus (AP 2.5 mm posterior to the bregma, ML 2.5 mm from the midline and DV 1.6 mm below the dura). The cannulae were implanted at an angle of 30° in the sagittal plane, with their tips pointing in the posterior direction to maximize the distribution of muscimol in the dorsal hippocampus. A jeweler's screw fixed to the skull served as a ground electrode for the recording electrodes. Microdrives and cannulae were secured to the skull using jewelers' screws and dental cement.

Data collection and hippocampal inactivation. The rats collected crumbs of vanilla or chocolate biscuit thrown randomly into a 50 cm–high square metal box with a black floor and black walls. The width of the square box was 100 cm for six rats and 150 cm for 5 of the 11 experiments with two rats (the remaining 6 experiments with two rats were in the 100-cm box). The box was polarized by a white cue card (45 cm × 50 cm) placed centrally on one of the walls. Curtains were not used, except for in three experiments in the larger box. The boxes were kept in a constant location. Between trials, the rat rested on a towel in a large flowerpot on a pedestal or in its home cage.

Electrophysiological data and position were recorded by connecting the microdrives to the recording equipment (Axona) using AC-coupled unity-gain operational amplifiers close to the rat's head, as well as a counterbalanced cable that allowed the rat to move freely within the available space. Over the course of 10–20 d, the tetrodes were lowered in steps of 50 µm or less until multiple well-separated theta-modulated large-amplitude low-frequency neurons appeared at depths of about 2.0 mm or more in the dorsolateral MEC or in area CA1 of the hippocampus. When the signal amplitudes exceeded approximately four times the noise level (r.m.s., 20–30 µV) and the units were stable overnight, data were recorded during foraging in the box.

Recorded signals were amplified 7,000×–25,000× and band-pass filtered between 0.8 kHz and 6.7 kHz. Triggered spikes were stored to disk at 48 kHz (50 samples per waveform, 8 bits per sample) with a 32-bit time stamp (clock rate at 96 kHz). EEG readings were recorded single ended from one or several of the electrodes in layer II or III of the MEC. The EEG readings were amplified 5,000×–10 000×, lowpass filtered at 500 Hz, sampled at 4,800 Hz and stored with the unit data. Movement was tracked with two light-emitting diodes (LEDs), one large and one small, 5–10 cm apart, that were fixed on the head stage connected to the microdrives. The tracking rate was 50 Hz.

The effect of hippocampal output on spatial firing in the MEC was tested by inactivating the hippocampus by local infusion of the $GABA_A$ receptor agonist muscimol (Sigma)[25]. On the test day, between 3 and 8 weeks after the start of training, place cells and grid cells were first recorded for 20 min (two consecutive blocks of 10 min) in the open field in the absence of the drug. Muscimol dissolved in PBS (pH 7.4; 0.5 µg µl^{-1}) was then infused into the two hippocampi using two 33-ga internal cannulae (C315I, Plastics One), each connected by polyethylene tubing to a 25-µl syringe mounted in a CMA/100 infusion pump. The tip of the internal cannulae protruded 0.9 mm beyond the implanted guide cannula. The infusion rate (0.08 µl per min) was controlled by the syringe pump. The total volume of each hippocampal infusion was 0.24–0.30 µl. The internal cannulae were retracted 2 min after the infusion. Left and right infusions were performed in parallel in all rats except rat 11468, which received left and right infusions at an interval of 7–10 min. Between 5 and 30 min after the infusions were completed, the rat was placed back in the open field for up to 160 min of additional parallel recordings from the hippocampus and the MEC. The after-infusion recording was performed either as a series of 10-min trial blocks with a 20–30 min break in the home cage after the third and fifth blocks or as three consecutive blocks of 30 min. The rat was then brought back to the vivarium, ~5 m away, and then returned to the recording box for two additional 10-min trial blocks 6 h or 24 h after the drug infusion. No drug was infused in the latter trials. After the 24-h trial, the tetrodes were moved further (50 µm or more) until new well-separated grid cells with new firing locations were encountered in the box, and the drug experiment was repeated. Individual rats were drug tested between two and ten times. Experiments were excluded from analysis if the rates were not reduced to 10% within 30 min (n = 3 trials).

The distribution of muscimol was estimated in a separate experiment in which four anesthetized rats received hippocampal infusions of FCM (**Supplementary Fig. 3**)[26]. One milligram of FCM was dissolved into 2 ml of 0.01 M PBS. The infusion protocol was similar to the one used for the rats with tetrode recordings (same cannula locations, same volume and same injection rates), but instead of first implanting an outer cannula, the inner cannula was inserted directly into the brain. After infusion, the inner cannula was left in place for 10 min. Moreover, the two hemispheres were infused separately, one 60 min and one 20 min before the rats were killed and perfused transcardially with formaldehyde. Anesthesia was induced and maintained with isoflurane (induction chamber level of 5.0% with an air flow of 1,200 ml per min gradually reduced to 1% after the rats were secured in the stereotaxic apparatus). The rats remained under anesthesia until perfusion. Levels of anesthesia were monitored regularly by testing toe and tail pinch reflexes.

Spike sorting and rate maps. Data were analyzed separately for blocks of 10 min before and after muscimol infusion. The number of cells per 10-min block decreased as a function of time after muscimol infusion. Spike sorting was performed offline for each block using graphical cluster-cutting software (*tint*, Neil Burgess and Axona). Position estimates were based on tracking of one of the LEDs on the head stage. Only epochs with instantaneous running speeds of 2.5–100 cm s^{-1} were included. To characterize firing fields, the position data were sorted into 2.5 cm × 2.5 cm bins, and the path was smoothed with a 21-sample boxcar window filter (400 ms, ten samples on each side). Firing-rate distributions were determined by counting the number of spikes in each bin and measuring the time spent per bin. Maps for the number of spikes and occupancy time were smoothed individually using a quasi-Gaussian kernel over the 5 × 5 bins surrounding each bin in the rate map[28]. Firing rates were determined by dividing the spike number and time for each bin of the two smoothed maps. Peak rate was defined as the rate in the bin with the highest rate in the smoothed firing-rate map. Spatial coherence was estimated as the mean correlation between the firing rate of each bin and the averaged firing rate in the eight adjacent bins[43]. Spatial coherence was calculated from unsmoothed rate maps.

Downsampling (**Fig. 5c**,**d**) was performed by random sampling of spikes from 10-min blocks of baseline data. For each cell, spikes were downsampled to mean rates of 2 Hz, 1.5 Hz, 1 Hz, 0.5 Hz and 0.1 Hz, and grid scores and mean vector lengths were computed for each case.

Analysis of grid cells. The structure of the rate maps was evaluated for all cells with more than 100 spikes in the baseline trial by calculating the spatial autocorrelation for each smoothed rate map[8,28]. The degree of spatial periodicity (grid score) was determined for each recorded cell from a series of expanding circular samples of the autocorrelogram, each centered on the central peak but with the central peak excluded[8,28]. The radius of the central peak was defined as either the first local minimum in a curve showing correlation as a function of average distance from the center or as the first incidence where the correlation was <0.2, whichever occurred first. The radius of the successive circular samples was increased in steps of one bin (2.5 cm) from a minimum of 10 cm more than

doi:10.1038/nn.3311

the radius of the central peak to a maximum of 10 cm less than the width of the box. For each sample, we calculated the Pearson correlation of the ring with its rotation in α degrees first for angles of 60° and 120° (group 1) and then for angles of 30°, 90° and 150° (group 2). We then defined the minimum difference between any of the elements in group 1 and any of the elements in group 2. The cell's grid score was defined as the highest minimum difference in the entire set of successive circular samples.

A cell was defined as a grid cell if its grid score exceeded a chance value determined by repeated shuffling of the experimental data[8,28]. Shuffling was performed for each cell individually with 400 permutations per cell. For each permutation, the entire sequence of spikes fired by the cell was time shifted along the rat's path by a random interval between a lower limit of 20 s and an upper limit of 20 s less than the length of the trial, with the end of the trial wrapped to the beginning. A rate map and a spatial autocorrelation map were constructed for each permutation, and a grid score was calculated. The distribution of grid scores was determined for the entire set of permutations for all 222 grid cells that were shuffled, yielding a total of 88,800 permutations. If the grid score from the recorded data was larger than the 95th percentile of grid scores in the distribution from the shuffled data, the cell was defined as a grid cell (**Supplementary Fig. 5**). The spacing of the grid cell was defined as the radius of the circular sample from the autocorrelation map that gave the highest grid score.

Analysis of head-direction cells. The rat's head direction was calculated for each tracker sample from the projection of the relative position of the two LEDs onto the horizontal plane. The directional-tuning function for each cell was obtained by plotting firing rate as a function of the rat's directional heading, divided into bins of 3° and smoothed with a 30° mean window filter (five bins on each side)[28]. The preferred firing direction was defined by the mean vector of the directional-tuning function. Directional stability was estimated by angular correlation across trial blocks of the distribution of firing rates over directional bins.

Head direction–modulated cells were defined as cells with mean vector lengths significantly exceeding the degree of directional tuning that would be expected by chance[28]. Threshold values were determined by a shuffling procedure performed in the same way as for grid cells and using a similar number of permutations per cell. Cells were defined as directionally modulated if the mean vector from the recorded data was longer than the 95th percentile of mean vector lengths in the distribution generated from the shuffled data.

Theta rhythm and modulation. Local EEG recordings were filtered offline using an acausal (zero phase shift) FFT bandpass filter[25]. The filter function was constructed using a Hamming window. For the low cutoff frequencies, 5 Hz and 6 Hz were chosen for the stopband and passband, respectively; 10 Hz and 11 Hz were chosen for the high passband and stopband cutoff frequencies, respectively. Theta modulation of individual neurons was determined from the FFT-based power spectrum of the spike-train autocorrelation functions of the cells. Cells were defined as having a peak in the theta frequency band if the peak of power in the 6–11 Hz band was higher than the peak in the 2–6 Hz band.

Histology and reconstruction of recording positions. Electrodes were not moved after the final recording session. The rats received an overdose of pentobarbital and were perfused transcardially with 0.9% saline and then 4% formaldehyde. The brains were extracted and stored in 4% formaldehyde. At least 24 h later, the brains were quickly frozen, cut in sagittal sections (30 µm) using a cryostat, mounted and stained with cresyl violet. All sections in the area of the tetrode trace were retained. For some brains, only every third section was used for cresyl violet staining. The positions of the tips of the recording electrodes were determined from digital pictures of the brain sections. The measurements were made using AxioVision (LE Rel. 4.3). The laminar location of the recording electrodes in the MEC was determined on the basis of cytoarchitectonic criteria[8].

Statistics. When not otherwise indicated, Student's t tests were two tailed and based on the assumption of a normal distribution. Data from three or more independent groups were compared by analysis of variance.

Computational model. As in ref. 31, the spike rate, s_i, of neuron i is determined according to:

$$\tau \frac{ds_i}{dt} + s_i = g\left[\sum_j W_{ij} s_i + I + \alpha v_t \cos(\theta_t - \theta_i)\right]_+ \quad (1)$$

where $[\ldots]_+$ is the threshold-linear function, g is the gain, I is the constant external input, α is the velocity modulation, v_t is the speed at time t in m s^{-1}, θ_t is the head direction at time t, θ_i is the preferred direction of neuron i and W_{ij} is the strength of connection from neuron to neuron as defined by:

$$W_{ij} = W_0 \,\text{heaviside}\left[R - \sqrt{(x_i - x_j - l\cos(\theta_i))^2 + (y_i - y_j - l\sin(\theta_i))^2}\right] \quad (2)$$

where $x_i = 1\ldots N$ and $y_i = 1\ldots N$ represent the position of neuron i in a two-dimensional $N \times N$ neuronal sheet with periodic boundary conditions, l is the spatial offset, R is the radial extent of the connectivity and W_0 is a negative number representing the strength of the inhibitory interaction between connected neurons. The directional preference is patterned in $N \times N$ tiles of neurons with preferences $k\pi/2$, $k = 1, 2, 3$ (refs. 30 and 31).

In each trial, the activity pattern was initialized to a predetermined hexagonal pattern. The time-varying velocity and head directions were taken directly from the experiments. The simulation then consisted of integrating equation (1) with a 1-ms time step over 10-min paths taken from the experiments. We analyzed the firing rate of 50 randomly chosen neurons from each simulation. The trials were conducted by setting the value of the constant external input I to discrete values ranging from 0 to 6 and repeating the simulation. Grid scores and mean vector lengths were calculated from the rates found by simulating equation (1) and the definition used in the experimental analysis. For the analysis of the grid score, the rate maps were smoothed using a two-dimensional normalized convolution with the same quasi-Gaussian kernel as described above. The mean and s.d. of these scores can be seen in **Figure 8b**. The other variables in the model were held constant and are $\alpha = 1$, $W_0 = -0.015$, $l = 2$, $g = 1$, $R = 25$ and $N = 128$.

Approvals. The experiments were approved by the National Animal Research Authority of Norway.

43. Muller, R.U. & Kubie, J.L. The firing of hippocampal place cells predicts the future position of freely moving rat. *J. Neurosci.* **9**, 4101–4110 (1989).